Plasma Science and Technology

PAPER

Experimental investigation on upstream and downstream discharges in airflows

To cite this article: Desheng ZHOU *et al* 2018 *Plasma Sci. Technol.* **20** 125402

Plasma Sci. Technol. **20** (2018) 125402 (9pp) https://doi.org/10.1088/2058-6272/aadc05

Experimental investigation on upstream and downstream discharges in airflows

Desheng ZHOU (周德胜)[1], **Jingfeng TANG** (唐井峰)[2,3], **Ximing ZHU** (朱悉铭)[3], **Daren YU** (于达仁)[3] **and Chaohai ZHANG** (张潮海)[1]

[1] School of Electrical Engineering and Automation, Harbin Institute of Technology, Harbin 150001, People's Republic of China
[2] Academy of Fundamental and Interdisciplinary Sciences, Harbin Institute of Technology, Harbin 150001, People's Republic of China
[3] School of Energy Science and Engineering, Harbin Institute of Technology, Harbin 150001, People's Republic of China

E-mail: tangjingf@hit.edu.cn

Received 17 May 2018, revised 28 July 2018
Accepted for publication 13 August 2018
Published 20 September 2018

Abstract

Dielectric barrier discharge has widely used in airflow control, ignition and combustion, and other applications; the influence of airflow on dielectric barrier discharge is of extensive concern. Previous studies demonstrate that the discharge becomes more uniform and the discharge intensity decreases with increasing of airflow velocity. In this study, we adopt a discharge cell construction with upstream and downstream structure and study the discharge states and intensities. The experimental results demonstrate that within a specific range of airflow speed, the upstream discharge intensity is decreased, and the downstream discharge intensity is enhanced. The physical basis for this phenomenon is proposed as follows: Within a pulse interval time, some particles, such as charged and metastable particles produced by the upstream discharge, could be transported to the downstream region. The concentration of particles in the downstream region is increased, and these particles play a pre-ionization role in the downstream discharge, the intensity of the downstream discharge is enhanced. Further, factors such as the pulse frequency and the distance between electrodes are discussed in detail, along with the conditions for enhancing downstream discharge intensity.

Keywords: atmospheric pressure discharge, dielectric barrier discharge, airflow

(Some figures may appear in colour only in the online journal)

1. Introduction

Dielectric barrier discharge (DBD) has been considered as a non-thermal plasma source for many applications, such as airflow control [1, 2], and ignition and combustion [3, 4], and the coupling effect between airflow and discharge has been widely studied. Previous studies have shown that the discharge mode and intensities can be influenced by airflow. For example, Gherardi *et al* [5, 6] and Pavon *et al* [7] illustrate that transverse and laminar airflow of nitrogen in DBD could prevent a uniform glow discharge from transitioning to a filamentary discharge. They propose that gas flow would change the distribution of particles accumulated on the dielectric surface, leading to changes in the discharge characteristics. Pang *et al* [8] Liu *et al* [9] and Luo *et al* [10, 11] study unipolar repetitive nanosecond discharge in airflows at different velocities. They show that the discharge behaviors may be ascribed to the combined action of two different effects; one is the removing effect on the accumulated charge on the surface of the dielectric board, and the other is the loss of metastable particles under the forced convection of airflow. Tang *et al* [12, 13] and Ren *et al* [14–17] also discuss the effect of airflow on nanosecond pulse volume discharge. Their results show that the discharge becomes more diffuse, the discharge intensity decreases, and the breakdown voltage and time lag increase. Moreover, the temperature of the discharge plasma decreases when a small-velocity airflow is introduced into the discharge gap. These

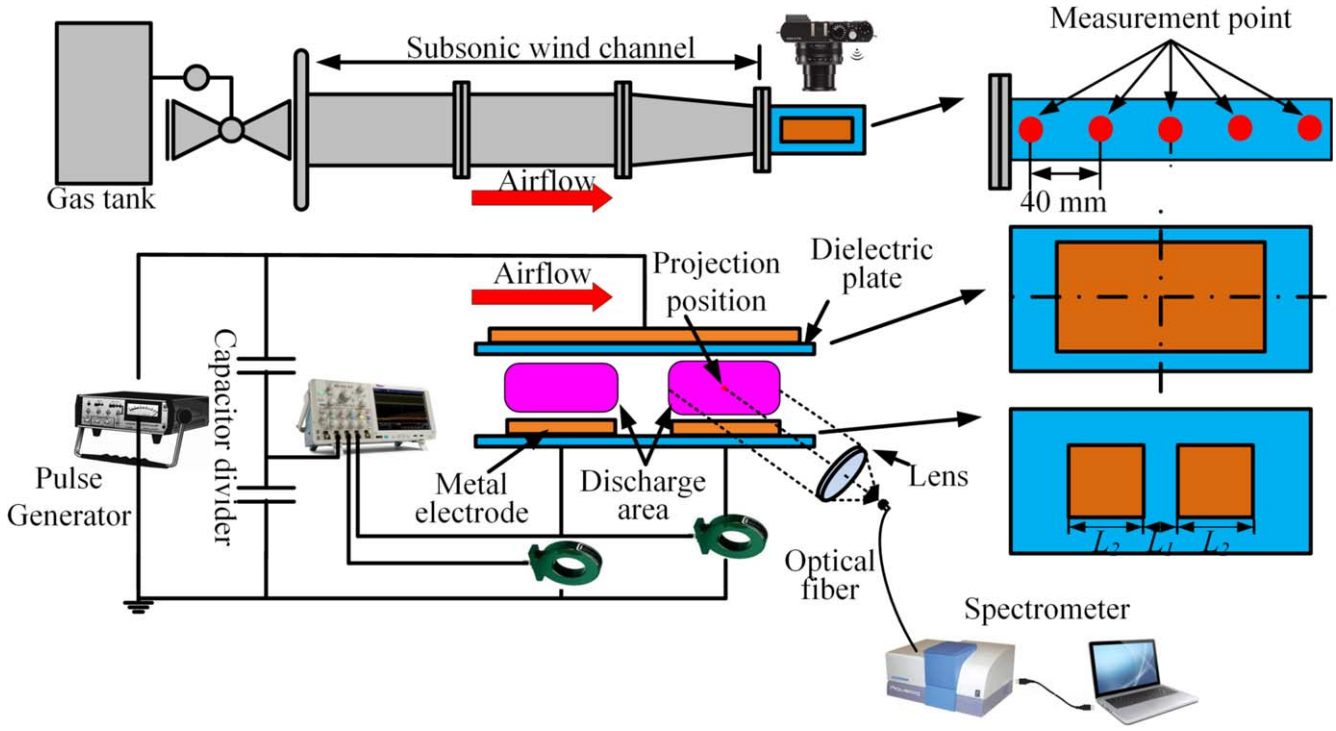

Figure 1. Schematic diagram of the experimental setup [12].

Table 1. Airflow velocities at different positions of plate slit.

Location	Speed test 1	Speed test 2	Speed test 3	Speed test 4	Speed test 5	Average Speed
Point 1	11 m s^{-1}	10 m s^{-1}	11 m s^{-1}	9 m s^{-1}	9 m s^{-1}	10 m s^{-1}
Point 2	31 m s^{-1}	30 m s^{-1}	31 m s^{-1}	30 m s^{-1}	28 m s^{-1}	30 m s^{-1}
Point 3	51 m s^{-1}	49 m s^{-1}	50 m s^{-1}	51 m s^{-1}	49 m s^{-1}	50 m s^{-1}
Point 4	71 m s^{-1}	71 m s^{-1}	68 m s^{-1}	71 m s^{-1}	69 m s^{-1}	70 m s^{-1}
Point 5	91 m s^{-1}	91 m s^{-1}	89 m s^{-1}	89 m s^{-1}	90 m s^{-1}	90 m s^{-1}

phenomena occur because the airflow changes the spatial distribution of particles in the discharge gap. Li *et al* [18], Uchida *et al* [19] and Liu *et al* [20], investigate the effects of flow rate on atmospheric pressure plasma jets. The results show that the length and uniformity of plasma jets could be adjusted by the flow rate; the metastable atoms of the flowing gas are possibly responsible for the plasma discharge. Darny *et al* [21], Robert *et al* [22] and Bradley *et al* [23] investigate the influence of gas flow on plasma jet, the results show that the density of particles could be adjusted by the airflow condition such as laminar and turbulence, and the relationship between airflow and pulse interval time would also influence the characteristic of plasma jets such as length and reactive species. The results demonstrate that the discharge state of DBD could be influenced by airflow, and the discharge intensity decreases with increased airflow velocity. In this study, a type of discharge device with an upstream and downstream structure is adopted, and the interactions between airflow and discharge are investigated. The experimental results show that within a range of airflow speed, the upstream discharge intensity decreases, and the downstream discharge intensity is enhanced. The physical basis for this phenomenon is suggested by analyzing the relationship between pulse interval time and airflow transport time. The particles motions are discussed, and the corresponding factors are also studied.

2. Experimental setups

A discharge device with a two-electrode structure is designed. Figure 1 shows the schematic diagram and includes a subsonic wind channel, a nanosecond-pulse power source, discharge systems, and measurement systems. By changing the airflow input pressure, the speed at the end of the wind channel could be adjusted from 0 to 120 m s^{-1}. The airflow velocities at different positions of plate slit are also measured by a pitot tube. Each velocity is measured at five times, and the average values are shown in table 1, in which the airflow velocity keeps almost the same in the discharge slits. The electrodes are composed of stainless steel plates with one size of 60 mm × 120 mm × 2 mm (covered by Alumina

ceramics) and two sizes of 30 mm × 30 mm × 1 mm (bare electrodes). The size of the Alumina ceramics is 80 mm × 180 mm × 1 mm, the gap distance is 5 mm. The discharge system is installed at the exit of the wind channel with the flow direction perpendicular to the electrode surface.

The applied nanosecond voltage pulses have an adjustable amplitude, a fixed pulse width of 10 ns, and a fixed rise time of 5 ns; the pulse repetition frequency (PRF) range is 1–3800 Hz. A capacitive voltage divider is connected to the high-voltage output as the voltage probe, and the ratio is approximately 2200. The discharge current is measured by two Pearson 6585 Rogowski coils with a response time of less than 1 ns. The discharge signals are transmitted by a shielded cable, and a digital storage oscilloscope (Tektronix 5024) placed in a shielded room is used to record the discharge signals.

Typical average luminous images are obtained from the side view by a Canon EOS 80D camera. Optical phenomena are recorded by a digital CCD (Synapse Model: 354308) and analyze by an FHR1000 spectrometer. The sensitive scope of the spectrometer ranged from 200 to 1000 nm, and the spectral resolution is 0.01 nm. The optical emission spectroscopy is schematically described from the lateral position of the discharge device. The discharge emission is collected by a lens into an optical fiber, and the lens is accurately located to project the discharge area into the optical fiber.

According to the discharge device of the upstream and downstream regions of the flow channel, the upstream and downstream discharges under airflow include the generation and transport of particle. The generation of particles is related to external pulse excitation and the movement of particles could be influenced by the transport effect of airflow. The pulse interval time is denoted as t_p, the distance between the upstream and downstream regions is L_1 (mm), the length of the electrode plate is L_2 (mm). When the airflow velocity can pass the length of L_1 during the pulse interval time, the particles generated in the upstream discharge area would enter into the downstream discharge area, and the corresponding velocity can be defined as v_{min}, where $v_{min} = L_1/t_p$. And when the airflow movement distance is $L_1 + 2 \times L_2$, the particles generated in the upstream discharge area would be blown out of the downstream area, and the corresponding velocity can be defined as v_{max}, where $v_{max} = (L_1 + 2 \times L_2)/t_p$. Therefore, for a fixed pulse interval time t_p, when the airflow velocity v is less than v_{min}, the particles generated by the upstream discharge region would not be transported to the downstream discharge region, and when the airflow velocity v is faster than v_{max}, the particles would be out of the downstream discharge region; in the velocity region of $v_{min} \leqslant v \leqslant v_{max}$, the particles could be transported from the upstream region to the downstream discharge region, which would enhance the downstream discharge intensity. So, in our experiment, the discharge characteristic under the boundary velocities are analyzed, and the experimental results are as follows.

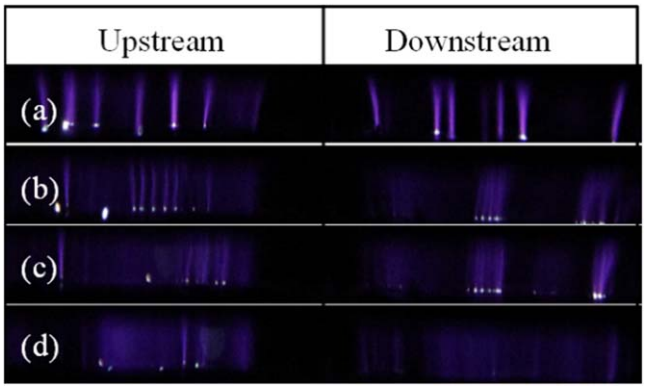

Figure 2. Discharge images at different velocities: (a) static air, (b) low speed ($v < v_{min}$), (c) medium speed ($v_{min} \leqslant v \leqslant v_{max}$), and (d) high speed ($v > v_{max}$).

3. Experimental results

In this study, we are experimentally analyzed the discharge characteristics of the upstream and downstream regions at different airflow velocities. Furthermore, different experimental conditions are employed to enhance the discharge intensity for the understanding of the mechanism.

3.1. Characteristics of upstream and downstream discharges

The PRF is 1 kHz and the distance between upstream and downstream is $L = 10$ mm, the maximum and minimum velocity (v_{max} and v_{min}) boundaries are $10\,m\,s^{-1}$ and $70\,m\,s^{-1}$, respectively. The discharge characteristics are studied at different airflow velocities.

The discharge images under different velocities are illustrated in figure 2, the exposure time is $1/200$ s.

As shown in figure 2(a), both the upstream and downstream discharge exhibit a filament discharge mode in a static condition of $v = 0\,m\,s^{-1}$. A filamentary mode is exhibited, which the filamentary are vertical distribution in the discharge region. As shown in figure 2(b), for the $v < v_{min}$ case, more filament paths are curved along the airflow, and some parts of the discharge area become uniform in eyes, and this phenomenon is due to the change in the discharge operation mode. As shown in figures 2(c) and (d), the transition from the filamentary mode to the diffuse mode occurs when the airflow velocities exceed the minimum velocity, in which nearly the entire discharge area exhibits a uniform state. A similar phenomenon is reported in [14, 15].

The corresponding current waveform is shown in figure 3, the first sharp rise of current occurs when the electric field is strong enough, and some charges are deposited on the dielectric surface. As more charges are deposited, the electric field between the upper electrode and the charged surface is high enough to generate a new discharge on the dielectric, giving rise to a negative current peak. The phase difference between the voltage and the current signals is corrected by measuring the time that the voltage and current signals transmit in the cable. By using the method introduced in

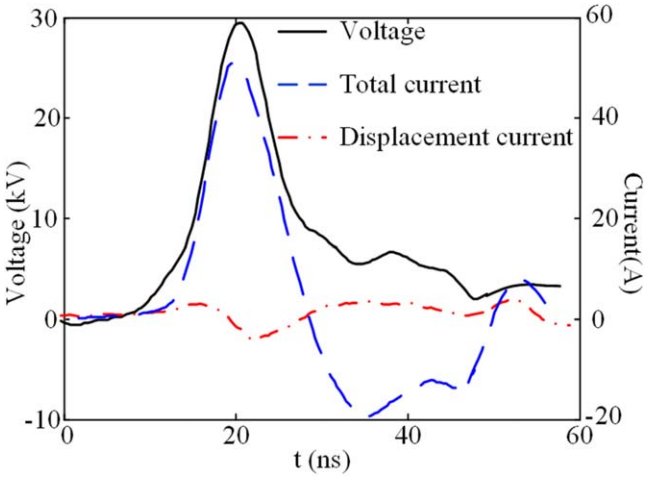

Figure 3. Voltage–current waveform.

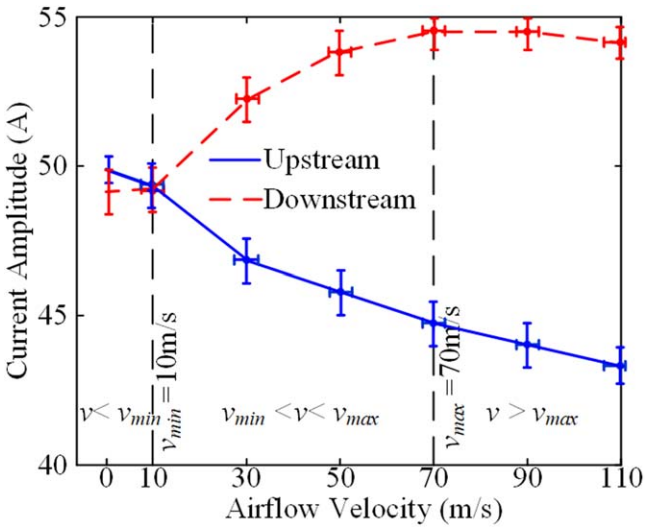

Figure 4. Amplitude of discharge current of the upstream and downstream regions.

[24–27], the displacement current and the conduction current are measured. It can be seen in figure 3, the amplitude of the conduction current (about 40−60 A) is much larger than that of the displacement current (about 3−6 A). Therefore, the conduction current is dominant in the discharge current.

Figure 4 shows the discharge current amplitudes for a PRF of 1 kHz under different airflow velocities. The current amplitude varies in a narrow range (upstream 48−50 A, downstream 47−49 A) in both the upstream and the downstream regions for the $v < v_{\min}$ case. For the condition of $v_{\min} < v < v_{\max}$, the current amplitude has a decrease of 6.3% (a decrease from 48 to 45 A) in the upstream region, and the downstream current exhibits an opposite trend (an increase from 48 to 54 A). The amplitude of the upstream discharge current keeps decreasing with the airflow velocity exceeding the $v_{\max}$, and the increase rate of the downstream discharge current tends to be zero.

For the PRF of 1 kHz, the emission spectra are measured in the upstream and downstream regions. Figure 5 shows the normalized emission spectra in the NPDBD (nanosecond pulse dielectric barrier discharge): The intensity of the emission spectrum in the upstream discharge has a decrease with the increase of the airflow velocity. It increases in the downstream discharge when the airflow velocity raises from $v_{\min}$ to $v_{\max}$.

The plasma temperature is calculated for further analysis of the characteristics of the upstream and downstream discharge. According to [15, 24, 25], due to the frequent collisions of the heavy particles and the small energy gap of rotational levels, the dynamic equilibrium between the rotational motions of N_2^+ and the translational motion of O_2 and N_2 is easily achieved. Therefore, the plasma temperature can be expressed by the rotational temperature of N_2^+, and the emission spectra of N_2 ($C^3\Pi_u \rightarrow B^3\Pi_g$) can be used to calculate the rotational temperature by comparing the experimental spectra with the calculated ones [28–30]. By using the code in [31, 32], the rotational temperature of N_2 is obtained by fitting the measured profile of the emission band (near 337.1 nm) with that of a simulated on, and the rotational temperature in the upstream and downstream discharges under airflow is shown in figure 6. It is about 380 K for the static-air condition and decreases to about 320 K for the condition of 80 m s^{-1} airflow velocity. While the gas temperature is substantially the same in the upstream and downstream regions, it is speculated that the gas temperature is not the key factor that determines the discharge intensity in the upstream or the downstream regions.

In summary, the mass transfer effect in the system plays a critical role in both the upstream and the downstream discharges at reasonable airflow velocities. The particles generated in the upstream discharge could be transported to the downstream discharge region, and the discharge is enhanced by the combined effect of flow transport and the pre-ionization of particles.

To further understand the mechanism of the downstream discharge, the relationship between the PRF and the distance between the upstream and downstream regions are explored in detail.

3.2. Experimental results under different pulse frequencies

The PRFs are adjusted to $f = 2$ kHz and 200 Hz, respectively. As shown in figure 7, for the 2 kHz pulse frequency, the minimum and maximum velocity boundary are 20 m s^{-1} and 140 m s^{-1}, respectively. Since less particles in the discharge can complete the diffusion and recombination process within the pulse interval time, the discharge intensity is increased as compared with the $f = 1$ kHz case. For the $v < v_{\min}$ case shown in figure 7, the current amplitudes of the upstream discharge slightly decrease from 55 to 53 A, while the downstream discharge has an increase from 51 to 53 A. The current amplitudes in the upstream discharge decrease gradually from 54 to 48 A at the medium speeds. That of the upstream discharge increase from 52 to 59 A. The $f = 200$ Hz provides an interval time of $t_p = 5$ ms, the velocity boundaries are $v_{\min} = 2$ m s^{-1} and $v_{\max} = 14$ m s^{-1}, respectively. The low PRF facilitates the diffusion and recombination process for the particle in the space, which reduces the

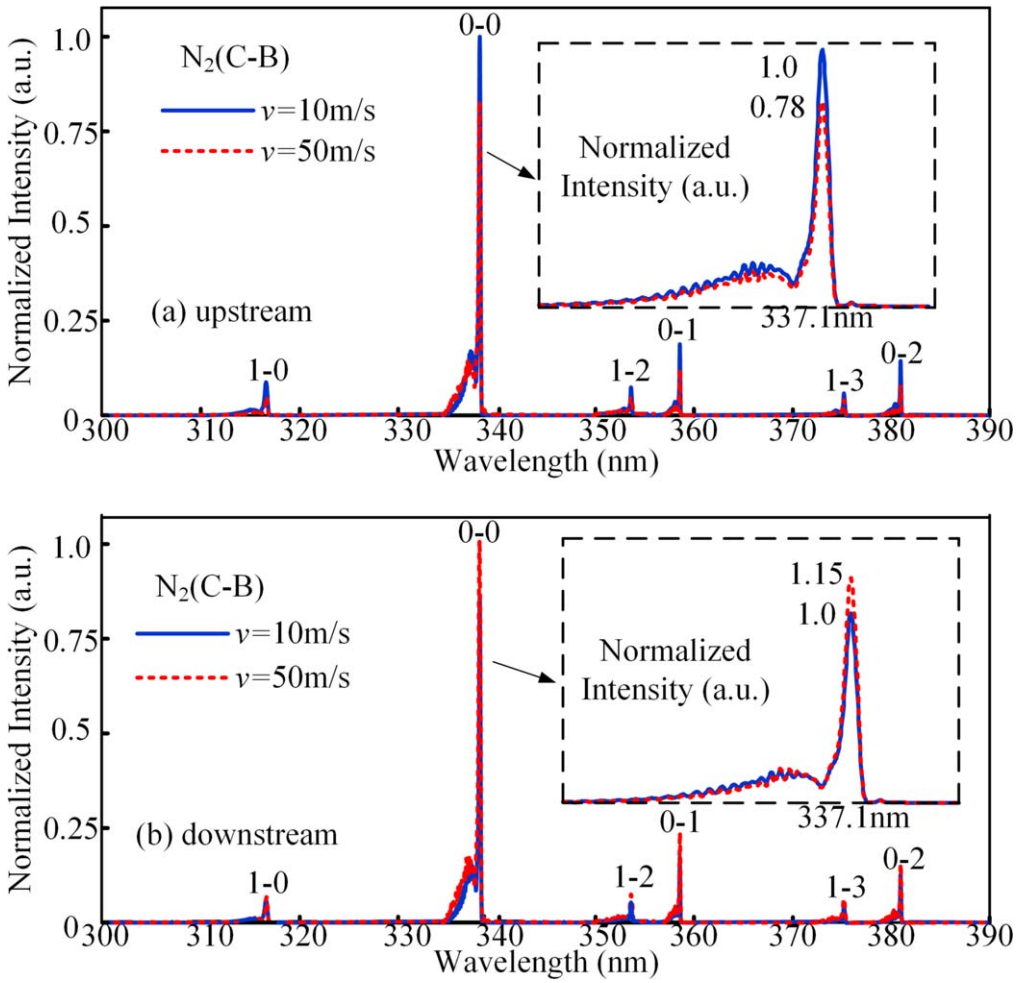

Figure 5. Normalized emission spectral intensity of discharge at different velocities: (a) upstream, (b) downstream.

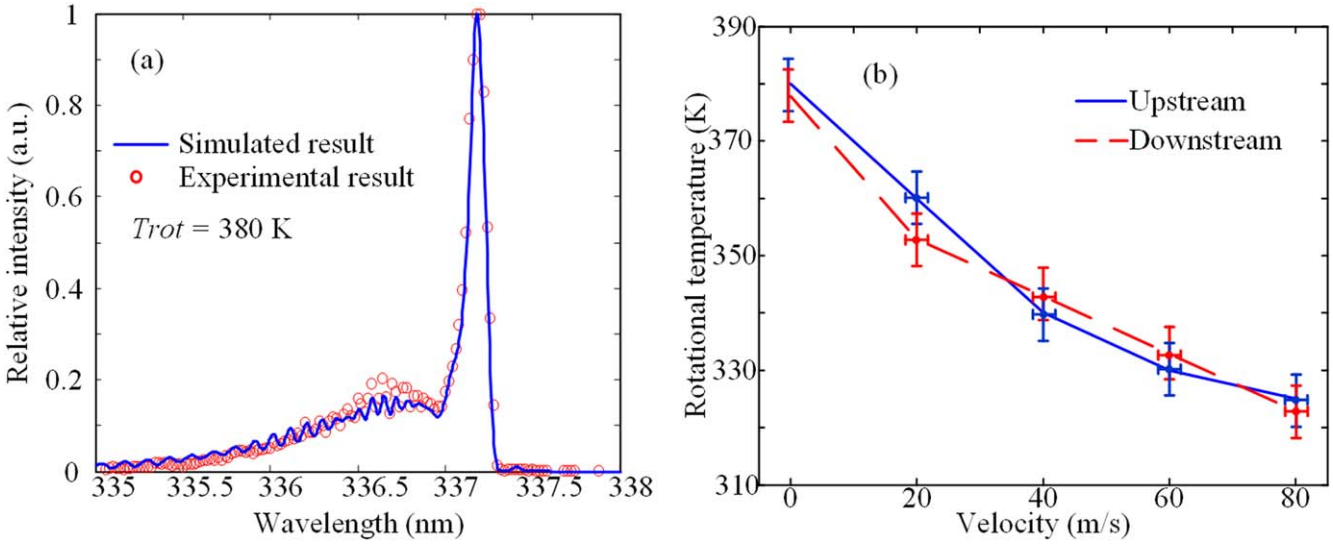

Figure 6. Rotational temperature at different velocities.

discharge intensity in the system. In the meantime, the current amplitude decreases from 46 and 43 A to 38 and 37 A for the upstream and downstream discharges when the airflow velocity in excess of the maximum velocity.

3.3. Experimental results under different distances between the upstream and downstream regions

The discharge is studied at distances (from the upstream to downstream regions) of $L_1 = 20$ mm and $L_1 = 50$ mm,

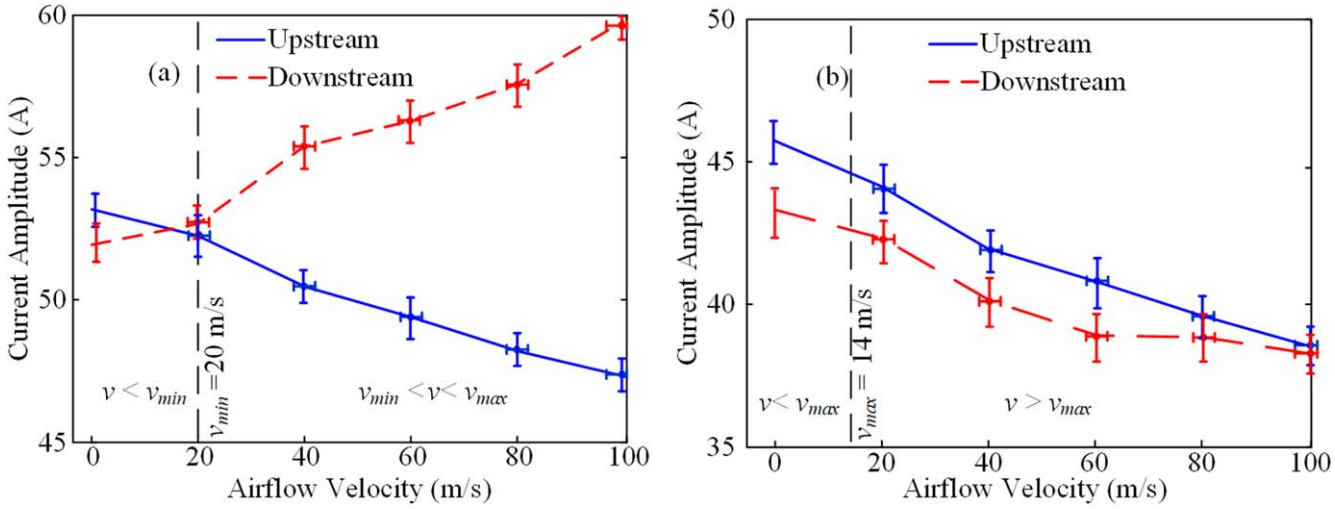

Figure 7. Amplitude of the discharge current at different pulse frequencies: (a) $f = 2$ kHz, (b) $f = 200$ Hz.

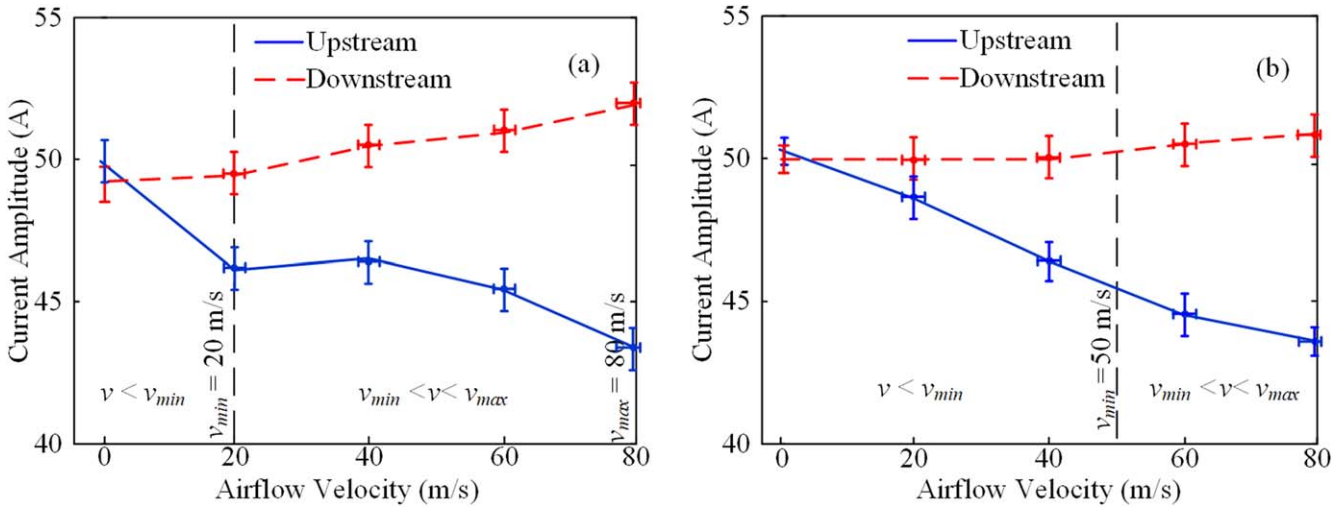

Figure 8. Amplitude of discharge current at different electrode distances: (a) $L = 20$ mm, (b) $L = 50$ mm.

respectively. The experimental results for $f = 1$ kHz are shown in figure 8. For $L_1 = 20$ mm, the velocity boundary is $v_{\min} = 20\ \mathrm{m\,s^{-1}}$ and $v_{\max} = 80\ \mathrm{m\,s^{-1}}$. for $v < v_{\min}$, the charged particles generated by the upstream discharge could not be transited to the downstream discharge region, the amplitude of the upstream discharge current would be decreased from 49 to 46 A, and the amplitude of the downstream discharge current fluctuates between 48 and 49 A. Particles generated in the upstream discharge region are carried to the downstream discharge region at medium velocities, which decreases the peak value of the upstream discharge current from 46 to 43 A and the current amplitude in the downstream discharge increases to 53 A correspondingly. A gas velocity of $50\ \mathrm{m\,s^{-1}}$ is reached when the distance between the electrodes is increased to 50 mm. The particles generated in the upstream discharge region could be transported to the downstream discharge region at such a high gas velocity. The peak value of the upstream discharge current would be decayed gradually from 51 to 44 A, and the downstream discharge current amplitude enhance slightly, the corresponding result as shown in figure 8(b).

4. Discussion

In this study, a discharge cell construction with upstream and downstream structure is designed. By matching the transport effect of airflow and the pre-ionization of particles, some of the particles generated by the upstream discharge could be transported to the downstream region, and those particles play a pre-ionization role in the downstream discharge, which causes the enhancement of the downstream discharge intensity. For the purpose of further recognizing the relationship between upstream and downstream discharge under airflow, the behavior of the particles is analyzed.

According to the process of pulse discharge, the electrons move to the anode under the effect of pulse voltage, and the ions remain nearly static in the time scale of nanoseconds; the

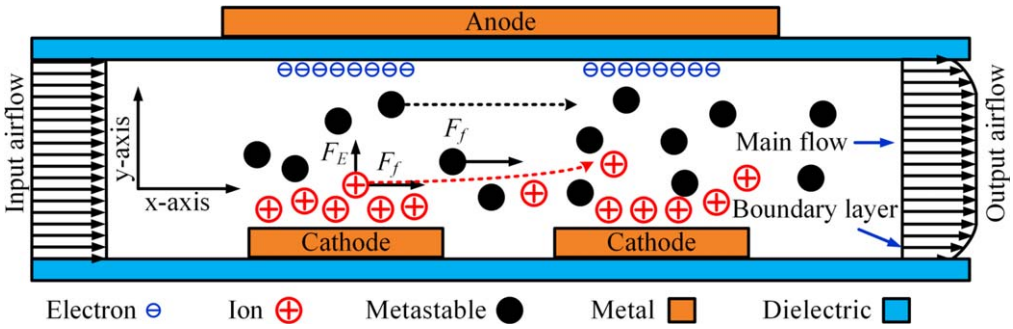

Figure 9. Schematic of particle motion paths.

discharge current is formed by electron migration. The electrons cover the surface of the dielectric, and a large number of ions are accumulated in the discharge space. At the falling edge of the voltage pulse, when the applied voltage potential is lower than the potential generated by the positive charge space, some electrons move towards the cathode and form a reverse current. During the movement, the electrons are neutralized with some positive ions and the concentration of positive charges declines in the space reduces.

Because of the different time scales of pulse discharge and airflow, the airflow cannot directly affect the process of pulse discharge. The rising time of the pulse discharge takes place in a few nanoseconds, and the duration of current is in the tens nanoseconds. For particles, the diffusion and recombination of neutral and charged particles takes place on a micro- and millisecond time scale, and the lifetime of the metastable particles produced by the discharge in short gaps are thought to have a significant high concentration of some hundreds of microseconds to milliseconds [8, 15, 32]. Therefore, the airflow could affect the distribution of particles during the pulse interval times.

When the airflow is applied in the discharge space, the distribution and movement of particles in the discharge region could be influenced by the airflow; a schematic of the particles motion paths is shown in figure 9, and the analysis is as follows.

According to [5, 8, 33–36], the dominant energy transfer process is the energetic electrons induce N_2 molecules to the electronically excited states. The excitation with electron-N_2 molecules have a relatively high cross section and a low excitation energy. N_2 electronically excited state particles are generated as the main type of excited particles with high concentration in discharge area. N_2 ($A^3\Sigma_u^+$) can be called as metastable particle with a long-life time during the discharge process [33, 34]. However, the metastable particles could be quenched in air by oxygen with a constant of 1.7×10^{-12} $cm^3\,s^{-1}$ at atmospheric pressure, the lifetime is on the order of 100 ns [35]. Therefore, for the pulse interval time of 1ms, most of the metastable particles would be disappeared, and just a small part of metastable particles might be transferred to the downstream region during the pulse interval time of millisecond.

For the charged particles in the discharge space, the generation and recombination process of charged particles would be participated in the discharge process. According to [36, 37], the charged nitrogen particles might be generated by the following chemical reaction during the discharge process

$$e + N_2 \rightarrow e + e + N_2^+, \quad (1)$$

$$N_2(A) + N_2(a') \rightarrow e + N_4^+. \quad (2)$$

The dissociative recombination reaction might be as follows:

$$e + N_2^+ \rightarrow N + N, \quad (3)$$

$$e + N_4^+ \rightarrow N_2(X,\ v = 0) + N_2(X,\ v = 0). \quad (4)$$

The recombination rate of N_2^+ and N_4^+ could be calculated by $\alpha = 2.8 \times 10^{-7} \times (300/T_e)^{1/2}$ $cm^3\,s^{-1}$ and $\alpha = 2 \times 10^{-6} \times (300/T_e)^{1/2}$ $cm^3\,s^{-1}$. The electron temperature T_e could be as estimated a few tens electron volt [14]. For the pulse interval time of 1ms, the retained ions density might be about several tens of initial ions density. These charged ions would be transferred to the downstream discharge region during the pulse interval time, and these particles might be play a pre-ionization role to the downstream discharge.

The charged particles move along the airflow direction mainly under the effect of the drag force of airflow and the electrostatic force from the surface electrons [15, 16]. According to the literatures [38–42], during a pulse interval time of approximately 1 ms, the electric field strength between the surface electrons and the space charged particles is about several $kV\,cm^{-1}$, and as shown in [9], when the gas flow applied to the discharge area, the magnitude of peak density reduced nearly two orders, and the charged ions density n_i under airflow during the pulse interval time is approximately from 10^7 to 10^8 cm^{-3}, the electric field force F_E of ions can be written as $F_E = qn_iE$ [9, 39, 40]. The estimated electric field force of the charged particles per unit volume is approximately from several to dozens of $N\,m^{-3}$.

In terms of the bulk flow, the conservation of momentum of the bulk fluid is described by the Navier–Stokes equation:

$$\rho\frac{d\vec{v}}{dt} = -\nabla p + \mu\nabla^2\vec{v}, \quad (5)$$

where v is the velocity of the bulk gas, ∇p is the pressure gradient, and μ is the gas viscosity, ρ is the air density. The air density is approximately $1.29\,kg\,m^{-3}$, the volume of the discharge area is approximately 5 mm × 30 mm × 70 mm, and the pressure difference between inlet and outlet is nearly 0.1% of the atmospheric pressure, so the estimated flow field force F_f to the charged particles per unit volume is approximately hundreds of $N\,m^{-3}$, and the flow force is much bigger than the

electrical field force during the pulse interval time [43]. For the charged particles in the middle region of the gap, during the pulse interval time of approximately 1ms, the distance of charged particles moved along the y-axis is much less than the gap distance; the estimate calculation illustrates that the ions could be blown to the downstream area during the pulse interval time under the coupling force of the airflow and electric field. Furthermore, the charged particles in space have different velocities at different regions in the airflow channel. In the region near the dielectric, the charged particles in space have a lower velocity because of the drag force in the boundary layer and the larger electrostatic force from the surface electrons. However, the charged particles in space in the middle region of the gap have the fastest velocities and the smaller electrostatic force, and the drag force from the airflow plays a dominant role compared with the electrostatic force of the surface electrons. The curved discharge channel under the low-speed condition also illustrates that the effect of the drag force from the mainstream area is stronger than the electrostatic force; this phenomenon is also discussed in the literature [15].

Therefore, both the estimation results and the discharge phenomenon illustrate that some particles, such as metastable particles and charged particles, could transmit to the downstream discharge area during the pulse interval time; these particles could play the pre-ionization role to the downstream discharge, and the downstream discharge intensity is enhanced.

The discharge states and intensities of the upstream and downstream discharges under different corresponding factors were investigated. The experimental results show that when the PRFs are $f = 1$ kHz and $f = 2$ kHz, the enhancing effect of downstream discharge intensity can be achieved by reasonably matching the airflow velocity. For the condition of $f = 200$ Hz, most of the particles in space complete the diffusion and recombination process during the pulse interval time, and the discharge intensity is reduced. Furthermore, most of the particles generated by the upstream discharge are blown out of the downstream discharge under the pulse interval time; the effect of pre-ionization is decreased, and the enhancement effect of the downstream discharge is not obvious.

For a fixed pulse frequency $f = 1$ kHz, by adjusting the distance between the upstream and downstream regions, the corresponding matching airflow velocities are different, the enhancement effect is inconsistent, and the interactions between airflow and discharge are different. For $L = 20$ mm, the downstream discharge intensity obviously increases when the matching relation of $v_{\min} < v < v_{\max}$ is satisfied. However, when the distance $L = 50$ mm, and the matching airflow velocity range adjusts from $v_{\min} = 50\,\mathrm{m\,s^{-1}}$ to $v_{\max} = 120\,\mathrm{m\,s^{-1}}$, the enhancement effect is not obvious, which may be attributed to two reasons. One is that the upstream discharge intensity at $v_{\min} = 50\,\mathrm{m\,s^{-1}}$ is lower than that of the conditions $v_{\min} = 10\,\mathrm{m\,s^{-1}}$ and $v_{\min} = 20\,\mathrm{m\,s^{-1}}$; another is that the forced convection of the airflow is enhanced, and this effect is unfavorable for the enhancement of discharge intensity.

5. Conclusions

In this study, by using a type of discharge device with upstream and downstream structure, the transport effect of airflow is studied. The results show that the upstream discharge intensity is decreased, and the downstream discharge intensity is improved; the interactions between airflow and discharge were explored, and the corresponding influencing factors were analyzed.

(1) With increasing airflow velocity, both the upstream and downstream discharge become more uniform in eyes. The upstream discharge intensity is weakened, and for the downstream discharge, the discharge intensity exhibits an increasing trend under the matching condition of $v_{\min} < v < v_{\max}$.
(2) The behavior of particles was analyzed. Under the effect of airflow, by reasonably matching the relationship $v_{\min} < v < v_{\max}$, particles generated by the upstream discharge, such as charged and metastable particles, could be transported to the downstream discharge region, and play a pre-ionization role to the downstream discharge, the downstream discharge intensity is improved. Furthermore, the influences of PRF f and electrode spacing L_1 to the downstream discharge intensity are examined. The results show that the initial conditions such as pulse frequency and the distance between electrodes could also affect the enhancement effect of downstream discharge.

Acknowledgments

This work is supported by National Natural Science Foundation of China (Grant Nos. 51437002, 51676053).

References

[1] Bayoda K D, Benard N and Moreau E 2015 *J. Appl. Phys.* **118** 063301
[2] Riherd M and Roy S 2014 *J. Phys. D: Appl. Phys.* **47** 125203
[3] Breden D *et al* 2013 *J. Appl. Phys.* **114** 083302
[4] Vincent-Randonnier A *et al* 2007 *Plasma Sources Sci. Technol.* **16** 149
[5] Gherardi N *et al* 2000 *Plasma Sources Sci. Technol.* **9** 340
[6] Gherardi N and Massines F 2001 *IEEE Trans. Plasma Sci.* **29** 536
[7] Pavon S *et al* 2007 *J. Phys. D: Appl. Phys.* **40** 1733
[8] Pang L *et al* 2011 *IEEE Trans. Plasma Sci.* **39** 2922
[9] Liu F C, Zhang D Z and Wang D Z 2010 *Phys. Plasmas* **17** 103508
[10] Luo H Y *et al* 2008 *J. Phys. D: Appl. Phys.* **41** 205205
[11] Luo H Y *et al* 2010 *J. Phys. D: Appl. Phys.* **43** 155201
[12] Tang J F *et al* 2014 *IEEE Trans. Plasma Sci.* **42** 753
[13] Tang J F, Wei L Q and Huo Y X 2016 *Plasma Sci. Technol.* **18** 273
[14] Qi H C *et al* 2016 *Plasma Sci. Technol.* **18** 520
[15] Qi H C *et al* 2016 *Phys. Plasmas* **23** 053509
[16] Fan Z H *et al* 2016 *Phys. Plasmas* **23** 123520

[17] Wang Z *et al* 2009 *Plasma Sci. Technol.* **11** 177
[18] Li Q *et al* 2009 *Appl. Phys. Lett.* **95** 141502
[19] Uchida G *et al* 2015 *IEEE Trans. Plasma Sci.* **43** 737
[20] Liu W Z *et al* 2017 *J. Phys. D: Appl. Phys.* **50** 415201
[21] Darny T *et al* 2017 *Plasma Sources Sci. Technol.* **26** 105001
[22] Robert E *et al* 2014 *Plasma Sources Sci. Technol.* **23** 012003
[23] Bradley J W *et al* 2011 *IEEE Trans. Plasma Sci.* **39** 2312
[24] Shao T *et al* 2011 *Plasma Sci. Technol.* **13** 735
[25] Shao T *et al* 2011 *Plasma Sci. Technol.* **13** 591
[26] Zhang C *et al* 2013 *IEEE Trans. Dielectr. Electr. Insul.* **20** 1304
[27] Gu J W *et al* 2016 *Plasma Sci. Technol.* **18** 230
[28] Song Y *et al* 2016 *Phys. Plasmas* **23** 083520
[29] Li X C *et al* 2013 *Acta Phys. Sin.* **62** 165205 (in Chinese)
[30] Stepanova V *et al* 2017 *Contrib. Plasmas Phys.* **57** 182
[31] Zhu X M and Pu Y K 2010 *J. Phys. D: Appl. Phys.* **43** 403001
[32] Wu Y *et al* 2008 *Appl. Phys. Lett.* **93** 031503
[33] Ono R, Nakagawa Y and Oda T 2011 *J. Phys. D: Appl. Phys.* **44** 485201
[34] Yu S *et al* 2016 *Phys. Plasmas* **23** 023510
[35] Herron J T 1999 *J. Phys. Chem. Ref. Data* **28** 1453
[36] Guerra V, Sá P A and Loureiro J 2004 *Eur. Phys. J. Appl. Phys.* **28** 125
[37] Kossyi I A *et al* 1992 *Plasma Sources Sci. Technol.* **1** 207
[38] Höft H, Becker M M and Kettlitz M 2016 *Phys. Plasmas* **23** 033504
[39] Ning W J *et al* 2017 *Phys. Plasmas* **24** 073509
[40] Hao Y P *et al* 2018 *Phys. Plasmas* **25** 013516
[41] Simeni M S *et al* 2018 *J. Phys. D: Appl. Phys.* **51** 01LT01
[42] Obradović B M, Ivković S S and Kuraica M M 2008 *Appl. Phys. Lett.* **92** 191501
[43] Pan J, Li L and Wang Y N 2016 *Plasma Sci. Technol.* **18** 1081